Proceeding of the IEEE
International Conference on Robotics and Biomimetics
Dali, China, December 2019

Design, Fabrication and Morphing Mechanism of Soft Fins and Arms of a Squid-like Aquatic-aerial Vehicle with Morphology Tradeoff

Taogang Hou[1], Xingbang Yang[1,2,3,4,*], Haohong Su[1], Lingkun Chen[1], Tianmiao Wang[1], Jianhong Liang[1], Siyang Zhang[1]

***Abstract*— Some animals have the ability to shuttle freely between water and air. These creatures have evolved special body structures to accommodate both underwater and airborne environments. Natural creatures have given us great inspiration to the variable structure design for aquatic-aerial multimodal vehicle. In this paper, we propose a new squid-like soft morphing fins according to the flying squid. This squid-like soft morphing fins can spread and fold for the adaptation of the aquatic-aerial multimodal locomotion. When the fin is spread, it can generate lift force for the aquatic-aerial vehicle. When the soft fin is folded, it can reduce the drag force during the underwater movement. An unique air cavity inside the fin was designed as actuator to bend the soft fin. The fabrication method of the soft fin was introduced. The bending performance of the soft fin was analyzed by FEA simulation and tested by several experiments. Then, morphology tradeoff strategy of aquatic-aerial vehicle with soft morphing fins was investigated by the wind and water tunnel. The results demonstrate the soft morphing fins have fast actuating response and good deformability, which verifies the soft fin can help the aquatic-aerial vehicle to realize multi-modal locomotion.**

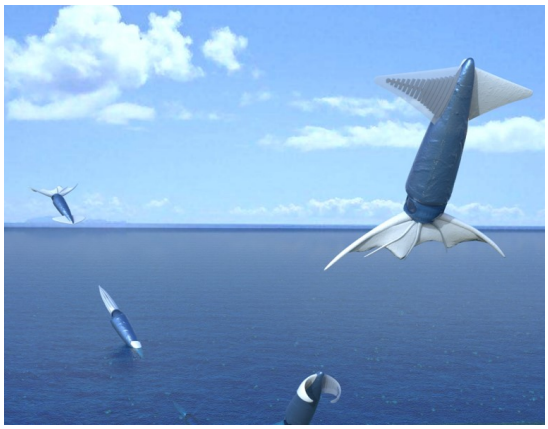

Fig. 1. Natural flying squid with the soft fins and arms can freely shuttle between water and air. Squid fins and arms in folded state when diving into water and spread when gliding in the air. The arm membrane forms a horizontal tail to have better fly performance.

I. INTRODUCTION

In nature, flying squid is a very special species among the aquatic-aerial amphibious animals that can freely realize water-air transition. The multi-locomotion of the flying squid can be divided into four steps: launching, jetting, gliding, and diving [1]. Its maximum velocity can reach up to 11.2 m/s or 43.9-49.7 BL(body length)/s [2], which is much faster than the ordinary fish [3]. When launching from the water, the speed of squid is able to reach about 10 m/s by jet propulsion [4], then it can fly about 26.4 m to 33.5 m in the air before diving into the water. It is greatly helpful to improve the performance of water surface takeoff of amphibious multi-mode aircraft by exploring the excellent multi-locomotion capability of flying squid and applying it to bionic design.

The research of water-air multi-locomotion theory and the fabrication of bionic prototype has been a hot spot in the world [5]. Researchers are inspired by animals with excellent aquatic-aerial characteristics in nature, such as gannet [6], [7], [8], seabirds [9], flying fish [3], [10], etc. Most of the existing achievements adopt traditional propeller propulsion and rigid structure, which reduces the bionic similarity and increases the weight and complexity of the structure. Therefore, it is not able to give full play to the advantages of the aquatic-aerial multi-locomotion.

With the advancement of material science, the research of soft robotics has brought substantial achievements [11]. Most of these robots are inspired by the natural mollusks with the ability to change their own structure such as octopus [12], [13], manta [14], and starfish [15], etc. Besides, some special soft structures can change their stiffness for specific operation [16], [17]. Compared with the rigid structure, the soft structure shows better elastic and deformable properties, which allows the soft robots to adapt various environment.

As shown in figure 1, the excellent aquatic-aerial multi-locomotion capability of flying squid is mainly due to its propelling mode and morphing structure characteristic of fins which adapt to multi-locomotion movement in water and air. In reality, flying squid can jet water to reach a high speed within a short time [18], [19], [20]. Later, it can expand the fins as wings and glide in the air. In order to simulate the flying squid's behavior and improve the performance of the bionic prototype, we proposed the application of soft robotics technology to the amphibious multi-locomotion aircraft.

In this paper, we present a realization about the aquatic-aerial vehicle's variable structure motion. In the following chapters, the paper discusses the design, the fabrication and

This research was supported by Beijing Municipal Natural Science Foundation grant number 3184054; the National Science Foundation of China grant numbers 61703023; China Postdoctoral Science Foundation (2016M600892 and 2018T110024); China Scholarship Council (grant no. 201706025021).

[1] Taogang Hou is a Ph.D. Candidate in Mechanical Engineering and Automation & Shenyuan Honors College, Beihang University.

[1,2,3,4,*] Xingbang Yang is with School of Mechanical Engineering and Automation, School of Biological Science and Medical Engineering, Beijing Advanced Innovation Center for Biomedical Engineering at Beihang University and the MIT Media Lab at Massachusetts institute of technology. Correspondence: xingbang@mit.edu

978-1-7281-6321-5/19//$31.00 ©2019 IEEE

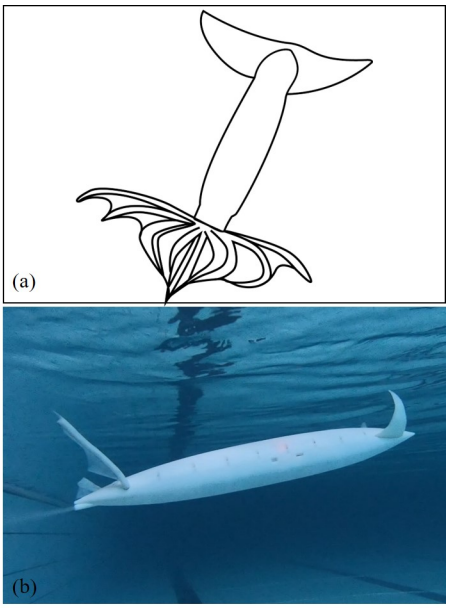

Fig. 2. (a) The overlooking view of airborne behavior of flying squid, which is spreading its fins and arms. (b) The squid-like bionic prototype being propelled by water jet flow underwater. Soft fins and arms are in spread state. The thruster inside the prototype body is not fully open and the swimming speed is around 0.5m/s.

the principle of soft fin, and proves the soft fin's excellent performance and the advantages of variable structure by simulation and physical experiments.

II. METHODS

A. Prototype and Variable Structure Design

The soft morphing squid-like prototype consists of pneumatic system, electric control system and body shell. The pneumatic system plays an important role in the squid-like prototype's moving performance and soft morphing actuator. It is necessary for the squid-like prototype to adopt jet propulsion unit, which uses compressed gas to produce jet-flow at the tail of the prototype. The compressed gas is stored in a gas cylinder and connected with a bionic mantle cavity, which is filled with water. When the prototype is propelled by the jet flow, the gas from gas cylinder is pressed into the bionic mantle cavity to push the water ejecting through the jet orifice. With the help of the electronic control system, the gas in the gas cylinder can push the prototype forward and make the body structure change. During propelling by the jet flow, the prototype needs enough water to produce propulsion force. In order to reduce the weight of the prototype, the water from external environment can be sucked into the built-in reservoir through a centrifugal pump.

The pneumatic and electric control system are placed inside the cavity of the squid-like prototype's body. In order to ensure the complete isolation between the body cavity and the external environment, a sealing ring is installed in the clamping slot that is settled between the upper and lower body shells. The prototype is made of photosensitive resin material with low density and high strength by 3D printing (SLA), reducing the weight of the prototype while increasing mechanical strength to withstands impact force.

The soft morphing squid-like prototype mainly relies on its soft morphing fins to realize the body variable structure. The fin consists of silicone rubber material and air chambers. Its pneumatic soft actuator is made by soft material, and therefore the soft fin has excellent bending ability. When actuated, the gas gushes into one side of the air chambers, the inflated side of the soft fin can present outstanding ductility, and the other side will be bended as a solid part with poor ductility. The air chamber's expansion results in the preferential elongation of the former. Meantime, the latter extends little and has to bend to adapt the air chamber's larger deformation. If the other side is actuated, the soft fin can bend in the opposite direction. By controlling the pneumatic system, the prototype can realize the air chamber's inflatable expansion or not, which can enable the bionic prototype to fold or spread its pneumatic soft morphing fins. We can control the bending direction of the soft fin by choosing different air chamber. When jetting out of water, the soft fins can wrap around the body like a real flying squid. With the cooperation of soft morphing fins, pneumatic system and electric control system, the soft morphing squid-like prototype can copy the body variable structure of the natural flying squid successfully as shown in figure 2.

The appearance of the soft morphing squid-like prototype is very similar to the flying squids in nature. The length of the whole bionic prototype is 790 mm. Besides, the length of the soft morphing fin is designed as 200 mm, the maximum width of the soft morphing fin 85 mm, and the chord length is 193 mm. The suitable ratio of body and the soft fins makes the bionic prototype better mimic the actual movement of the flying squid in nature. The soft morphing fins use the concept of aircraft design theory. The whole cross section of the pair fin presents the structure of Clark airfoil [21], which can maximize the lift of flight when gliding in the air.

B. Fabrication

The fin of the soft morphing squid-like prototype is made of silicone rubber material ($Ecoflex^{TM}$ 00-30, Smooth-On Inc., America). The rigid molds are designed in SolidWorks (SolidWorks Corp., Waltham, MA, USA) and are made of photosensitive resin material by the 3D printer (SLA). The simplified process allows us to iterate the fabrication quickly.

The fabrication process of the soft morphing fin is given in figure 3. Firstly, the independent air chamber molds A and B are prepared and the uncured silicone rubber material is poured into the molds. Before pouring, the material should be placed in vacuum oven for to remove air bubbles. After silicone rubber material becoming solid, the independent air chambers are shaped. In addition, a quadrilateral silicone rubber layer is sealed with the independent air chamber for a complete air chamber. After that, we prepare the molds C and D to build the whole fin surface by a Two-Step casting procedure. Between the main soft fin molds, there is an inner mold for building another air chamber with topographical features. After the semi-finished soft fin is shaped, we get

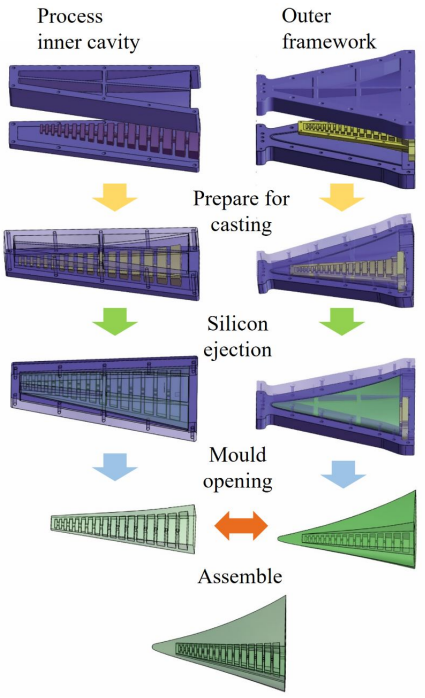

Fig. 3. The fabrication process of squid-like soft fins. Four steps, i.e., casting preparation, silicon gel ejection, mould opening and assembling, is adopted to fabricate the soft morphing fins, as well as the soft arms. The inner cavity (shown in left) and outer framework (shown in right) is processed separately.

it out of the molds and put the complete independent air chamber in it. By applying some silicone rubber glue, theses independent air chamber and the semi-finished soft fin can be firmly connected together. Finally, the soft fin is completed with a two-side, independent, multi-chamber system. By inflating one side of the air chambers, the soft morphing fin will bend in the other direction (as shown in figure 4), which further results in the soft fin's expansion or contraction.

C. Experiments

In order to optimize the fabrication procedure and obtain the shape of the fin and geometry parameter of inner chambers quickly, we simulate the variable structure characteristics of the fin. For the simulation conditions, finite element simulations are performed using the commercial software Abaqus (Abaqus 2018, Dassault Systèmes S.A., France). The soft morphing fin is modeled as an incompressible Yeoh material via the hyper elastic Yeoh model with the density (ρ) of 1.13 g/cm^3 and the material parameters (C_{10}, C_{20} and C_{30}) of 0.07, 0.012 and 0. For the elastomer, a 10-node quadratic tetrahedron element type is used with hybrid formulation (C3D10H). The accuracy of the mesh is ascertained through a mesh refinement study and a simplification of the model. Each simulation required 10509 elements and 17976 nodes. Quasi-static nonlinear simulations are performed using Abaqus/Standard. One end of the soft morphing fin is fixed both in the translation and rotation directions, and the pressure load is applied to the inner surface of the chambers. Unlike the direct simulation

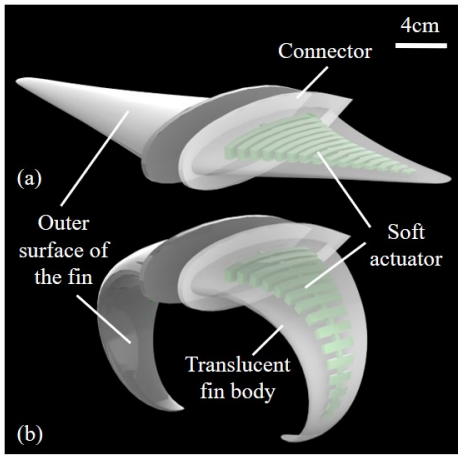

Fig. 4. The framework of soft morphing fins. The motion of the soft fins is controlled by the soft actuator (shown in the translucent view). (a) Spread state: the soft fins are spread, which often presents in the jetting and gliding phase. (b) Folded state: fins roll around the squid body, which can be found in the launching and diving phase.

of the soft morphing fin's bending, inertia has a great effect on the results after considering the inflation velocity. In order to obtain more accurate simulation data, it is necessary to use dynamic implicit nonlinear simulations.

After the fabrication of the soft morphing fin completed, a deformation experiment of the entity was carried out. The soft fin was fixed at base part and a list of marking points was made on the symmetrical midline in the front edge. The bending deformation of the soft fin was observed by controlling the different inlet pressure. A HD camera was used to record the whole process of the experiment for further study.

As for the whole soft morphing squid-like prototype, a wind tunnel experiment was conducted to investigate its performance in the air. The prototype was placed in the flow field generated by the wind tunnel and monitored by a high-frequency F/T(Force/Torque) sensor. We set the speed of the wind tunnel flow from 5 m/s to 15 m/s to simulate the speed of flying squid in air. Besides, experimental setup of underwater towing tank was used to test the performance of the prototype under water. The movement of the prototype can be provided by the towing platform. The prototype was connected to a 6-axis F/T sensor, which can record the three-axis force and the three-axis torque. Because maximum speed is limited by the underwater towing tank, the speed range of the experimental was set from 0.1 m/s to 0.6 m/s. The prototype was linked to a pneumatic system to control the spreading and folding of its soft fins during the experiment.

D. Theory

Hyperelasticity describes the behavior of elastomers under large deformation, which is often used in modeling soft material structures. In this paper, the silicone rubber material of the soft morphing fin can be regarded as a standard hyperelastic material. Hyperelastic materials are characterized

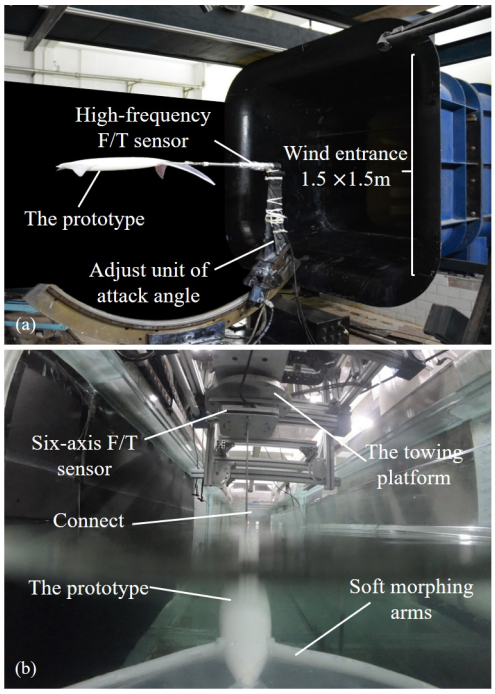

Fig. 5. (a) The experimental setup of wind tunnel test. A high-frequency Force/Torque sensor is used to test the performance of the prototype in the air and the adjust unit of attack angle can change the airborne attitude of the prototype. (b) The experimental setup of underwater towing test. The prototype is connected to a six-axis Force/Torque sensor and move in an accurate speed by the towing platform.

by a large strain energy density function $W(F)$. The stress resulting from deformation is:

$$P = \frac{\partial W(F)}{\partial F} \tag{1}$$

Where P is the first order Piola Kirchhoff stress tensor and F is the strain gradient tensor. From the *Cauchy*'s stress tensor σ and Piola Kirchhoff stress tensor, we can get:

$$PF^T = J\sigma \tag{2}$$

where J is the determinant of F, $J = det(F)$.

The energy stored in the hyperelastic materials only depends on the initial and final state of the deformation, and it is independent from the deformation path. Therefore, strain energy function is the simplest way to describe the stress-strain constitutive relation of hyper-elastic materials. According to different strain energy functions, the constitutive models of hyperelastic silicon rubber materials can be mainly divided into three types: Mooney-Rivlin model, Yeoh model and Ogden model, and the model's parameters can be obtained by experiment. In this paper, Yeoh model is used in the simulation. The strain energy function of the constitutive model is briefly introduced as follows [22]:

$$W = C_{10}(I_1-3) + C_{20}(I_1-3)^2 + C_{30}(I_1-3)^3 \tag{3}$$

Where C_{10}, C_{20} and C_{30} are the material parameters of hyperelastic silicon rubber, I_1 is the first invariant of left Cauchy-Green deformation tensor, W is the strain energy function determined by I_1.

λ_1, λ_2, and λ_3 are the elongation of three directions, which are the ratio of the specimen length after tensile to the initial specimen length. Hyperelastic silicone rubber materials can be considered as isotropic incompressible materials, so there is $\lambda_1\lambda_2\lambda_3 = 1$. During equiaxed tension, we order $\lambda_1 = \lambda_2 = \lambda_3$, then we can get $\lambda_3 = \frac{1}{\lambda^2}$. The above strain energy function can be simplified accordingly. The principal Cauchy stress σ_i is determined by the following formula [23]:

$$\sigma_i = \lambda_i \frac{\partial W}{\partial \lambda_i} - p, \quad i = 1,2,3 \tag{4}$$

where p is an arbitrary hydrostatic pressure introduced because of the incompressibility constraint. During tension, we can get:

$$p = \lambda_3 \frac{\partial W}{\partial \lambda_3} \tag{5}$$

According to the above formulas and the hypothetical conditions, it can be obtained that the relationship between Cauchy stress and Cauchy elongation of Yeoh model under the condition of equiaxed tension, which can be described as:

$$\sigma_{1,2} = 2(\lambda^2 - \lambda^{-4})[C_{10} + 2C_{20}(I_1-3) + 3C_{30}(I_1-3)^2] \tag{6}$$

where σ_1 and σ_2 are the Cauchy stress in the direction of two principal axes.

Considering the deviation between the finite element simulation and the deformation experiment of the entity, it is necessary to introduce the relative deviation as an authenticity reference. The formula is as follows:

$$\delta = \frac{\sqrt{\frac{1}{N}\sum_{i=1}^{N}(x_i - \bar{x})^2}}{L} \tag{7}$$

Where x_i is the deviation distance of the mark points between finite element simulation and the deformation experiment, $\bar{x}$ is the mean deviation distance of the mark points, and L is the size of the soft morphing fin. In order to simplify the calculation, the flying squid can be approximately regarded as a fixed-wing aircraft in the air. Similarly, same consideration are made in wind tunnel experiments. The lift and drag of flying squid in the air can be obtained as follows:

$$F_L = \frac{1}{2}\rho_a C_L v^2 S, \quad F_D = \frac{1}{2}\rho_a C_D v^2 S \tag{8}$$

Where ρ_a is the density of the air, C_L is the lift coefficient, v is the navigation speed, S is the reference area of the wing. The induced resistance coefficient C_D is obtained by the following formula:

$$C_D = \frac{C_L}{\pi A^2} \tag{9}$$

Where $A = L^2/S = L/b$ is the aspect ratio, which can be obtained by wing extension L and wing chord length b.

The lift coefficient can be obtained from the following formula [24]:

$$C_L = \frac{2\pi A}{2 + \sqrt{4 + \frac{A^2(1-Ma^2)}{\eta^2}(1 + \frac{tan^2\Lambda_{tmax}}{1-Ma^2})}} K_S K_F \tag{10}$$

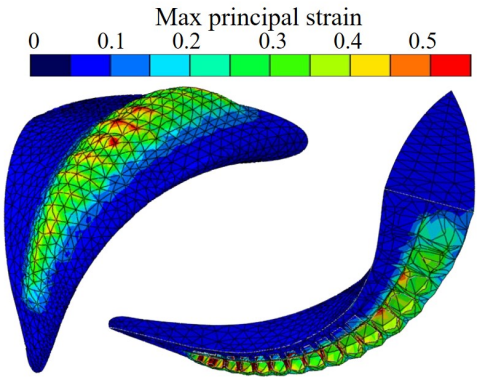

Fig. 6. Bending deformation simulation result for the soft morphing fin pressurized state at 196 kPa. The left shows the soft fin's bending deformation in a strain contour view that highlights the maximum principal strain locations. The right shows the strain distribution inside the soft fin.

Where η is the airfoil efficiency, Λ_{tmax} is wing swept angle , K_S is the parameter related to the wing area, K_F is the fuselage lift factor, Ma is Mach number. According to the above formulas, it can be obtained that the larger aspect ratio brings the higher lift and the lower drag.

III. DISCUSSION

A. Results

At the finite element simulation, we can get the simulation results of the soft fin bending process. The deformation stress diagram of the soft fin is illustrated in Fig. 6. When the soft fin is inflated, the stress concentration occurs at the connection of the upper and middle layers and the top of the air cavity. This phenomenon is in good agreement with the bending deformation experiment of the entity. Some marking points in the experiment video were marked in advance as reference, and the displacement data of the marker points in the bending process are obtained after the simulation.

When analyzing the video in the bending deformation experiment of the entity, we imported each image into software (MATLAB, MathWorks, America) to get the displacement data of the marker points. We have got three different pressure state from the experiment of the entity and the simulation. The results are brought into the equation (7) to calculate the reliability of the simulation. As shown in figure 7, the relative deviation of each set of results is less than 5% under the same pressure condition, and the simulation results are reliable.

While keeping the air pressure constant in the simulation, we change the increasing speed of the air pressure to observe the bending of the soft fin. It is possible to increase the inflatable velocity of the simulation process by changing the increase time of the peak pressure. As shown in Fig. 8, the simulation results show obvious lag compared with the pressure saturation time (The time when the pressure rises to the maximum). When the pressure reach maximum, the fin in the bending deformation simulation doesn't reach maximum deformation. The delay time is considered as the lag between the time when the fin spreading and the pressure

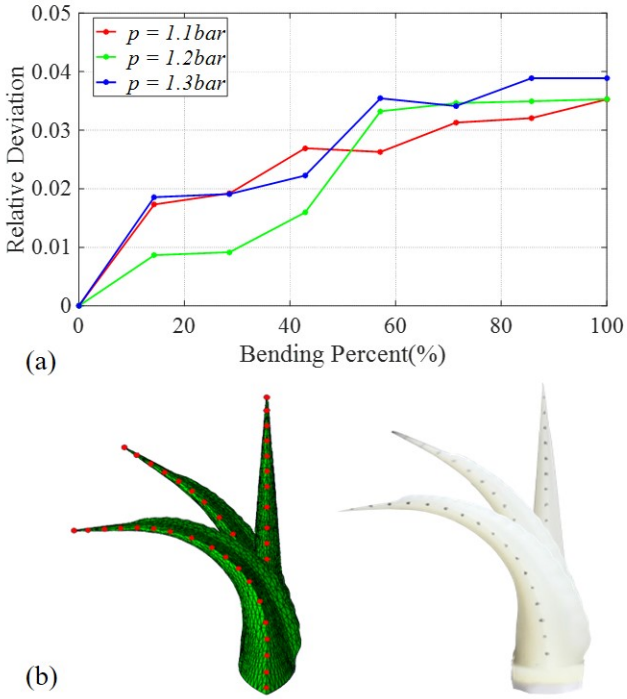

Fig. 7. Kinematics comparison between simulation and experiment for the soft morphing fin. (a) The relative deviation profiles during bending progress at 110-130 kPa pressure state. (b) This panel presents bending deformation progress in simulation and experiment.

saturation time. When the pressure saturation time begins to decrease, the inflatable velocity is larger, and the delay time is larger. With the increase of pressure saturation time, the inflatable velocity decreases, and the delay time tends to be stable.

Airborne behavior of flying squid has been reported by Yamamoto, who observed flying squid and succeeded in taking a sequence of photographs of the entire flight process in the Northwest Pacific [2]. According to the photographs, the mantle length of flying squid is estimated to be 122-135 mm, and the fin is about 50-55mm long and 24-27mm wide. The aspect ratio of the flying squid in nature as well as our prototype can be calculated. The aspect ratio of the flying squid in nature is about 8.2, which is close to the prototype's. According to equation (8,9,10), the fins with larger aspect ratio bring higher lift to drag ratio for the prototype. This design of the prototype is more suitable for the roaming of air medium in theory.

Through wind tunnel experiment and underwater towing test, the force condition of flying squid-like prototype under two different media can be obtained. In the air, the lift of the prototype when the fin is spreading is greater than that when the fin is folding (as shown in figure 9). The larger the wind speed, the greater the lift. Under the water, the prototype folding its fins will contribute to smaller drag than spreading. Therefore, it is necessary for the prototype to fold its fins when launching from the water. While gliding in the air, the soft fins should spread to maintain a certain lift.

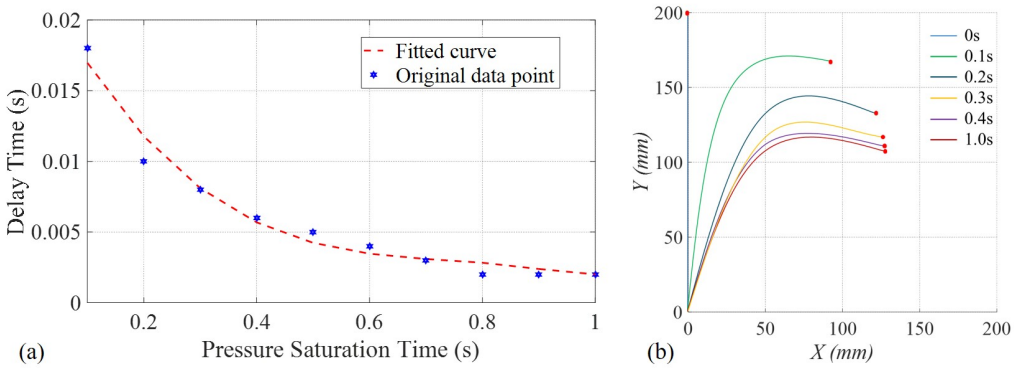

Fig. 8. (a) The influence of the pressure rising rate (Pressure saturation time) on the soft fin folding speed (delay time). The maximum pressure is set as 110 kPa. The greater saturation time, the slower pressure rise rate. (b) The tracks of the leading edge of the fins varies by pressure saturation time when the pressure reach maximum. The red dots denote fin tips.

B. Analysis

The reliability of the soft fin's bending simulation is verified by the experiments above. In order to optimize the shape parameter of the soft fin, we can use the finite element simulation to carry out some pretest of the soft fins' bending deformation. This will greatly speed up the iteration of the soft variable structure design and reduce manufacturing cost. It is proved that the inflation velocity affects the degree of spreading by the simulation experiments. As future work, we plan to further study the significance of the lag effect on the bending performance of the real soft fins.

In addition, the feasibility of the flying squid-like prototype's variable structure design is proved by wind tunnel experiment and underwater towing test. The prototype can expand the fins to obtain enough lift when flying in the air and fold its fins to reduce the roaming drag in the process of jetting acceleration. This also helps us to understand the advantages of flying squid's multimodal motion in nature.

IV. CONCLUSIONS

In this paper, we propose a new concept of soft morphing structure which can be used on the squid-like aquatic-aerial vehicle. The curling rubber actuator adopts soft pneumatic power, and its unique inflatable chamber helps soft morphing fin to spread and fold immediately. The folding mechanism and manufacturing method of the soft fins is introduced. The finite element simulation technique was used to optimize the soft-fin design to achieve better bending performance.

A deformation experiment of the real soft fin was implemented and compared with the simulation result. The results show that the design of the soft fin accords with the requirements of spreading and fast bending, which help the squid-like bionic prototype to realize water/air multi-locomotion. The force experiment of the prototype was carried out in wind tunnel and water tank, and the advantages of the body's variable structure in the aquatic-aerial flight have been verified.

In a word, this research combines the finite element analysis with soft structure design, which provides a new solution for the variable structure design of aquatic-aerial vehicle.

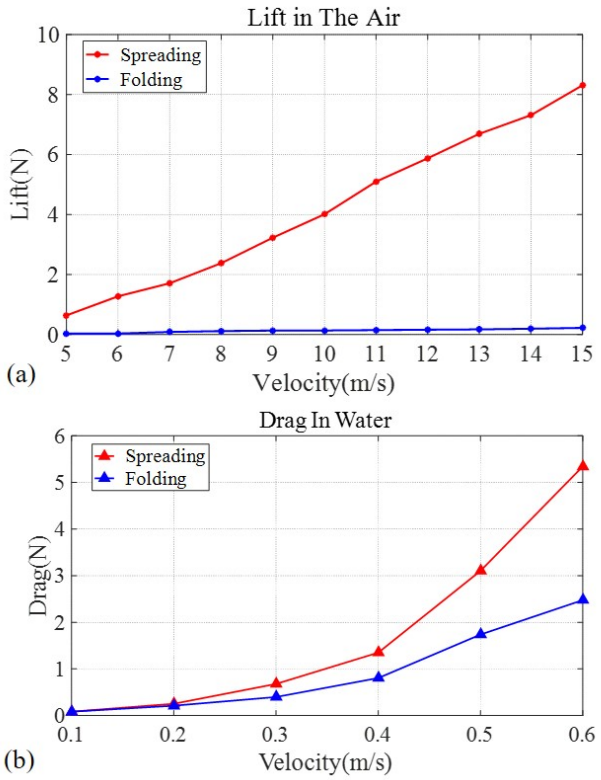

Fig. 9. The influence of the soft fins and arms on bionic prototype multi-locomotion investigated by wind tunnel and water tank. (a) Lift force of the prototype in the air when the air flow speed ranges from 5m/s to 15m/s with 1 m/s increment. (b) Drag of the prototype at 0° angle of attack in spread and folded state underwater, with a towing velocity between 0.1 and 0.6m/s in 0.1 increment.

ACKNOWLEDGMENT

We wish to thank Yunong Zhai for aiding the experiment setup. Buhui Jiang contributed to editing the manuscript. Thank Yang Liu's help in improving the English language.

REFERENCES

[1] R. O'Dor, J. Stewart, W. Gilly, J. Payne, T. C. Borges, T. Thys, "Squid rocket science: how squid launch into air," *Deep Sea Research Part II: Topical Studies in Oceanography,* (2013). 95, 113-118.

[2] K. Muramatsu, J. Yamamoto, T. Abe, "Oceanic squid do fly," *Marine biology,* 2013, 160(5): 1171-1175.

[3] A. Gao, A. H Techet, "Design considerations for a robotic flying fish," *Oceans,* 2011 (pp. 1-8). IEEE.

[4] R. O'Dor, S. N. Mendon, "Analysis of Sthenoteuthis oualaniensis flying behaviour from recorded video," *Cephalopod International Advisory Council Conference,* 2015, P13, 122.

[5] X. B. Yang, T. M. Wang, J. H. Liang, G. C. Yao, M. Liu, "Survey on the novel hybrid aquatic–aerial amphibious aircraft: Aquatic unmanned aerial vehicle (AquaUAV)," *Progress in Aerospace Sciences,* 2015, 74:131-151.

[6] T. M. Wang, X. B. Yang, J. H. Liang, G. C. Yao, W. D. Zhao, "CFD based investigation on the impact acceleration when a gannet impacts with water during plunge diving," *Bioinspiration biomimetics,* 2013, 8(3), 036006.

[7] J. H. Liang, G. C. Yao, T. M. Wang, X. B. Yang, W. D. Zhao, G. Song, Y. C. Zhang, "Wing load investigation of the plunge-diving locomotion of a gannet Morus inspired submersible aircraft," *Science China Technological Sciences,* 2014, 57(2):390-402.

[8] A. Fabian, Y. F. Feng, E. Swartz, "Hybrid aerial underwater vehicle," *Lexington: MIT Lincoln Lab,* 2012 SCOPE Projects, 2012.

[9] D. A. Shealer, "Foraging behavior and food of seabirds," *Biology of marine birds,* CRC press, 2001, 150-191.

[10] J. S. Izraelevitz, M. ST riantafyllou, "A Novel Degree of Freedom in Flapping Wings Shows Promise for a Dual Aerial/Aquatic Vehicle Propulsor," *IEEE International Conference on Robotics and Automation (ICRA),* pp. 5830-5837, 2015.

[11] T. G. Hou, T. M. Wang, H. H. Su, S. Chang, L. K. Chen, Y. F. Hao, L. WEN, "Review on soft-bodied robots," *Science & Technology Review,* 1985, 252(1): 96-103.

[12] M. Wehner, R. L. Truby, D. J. Fitzgerald, et al, "An integrated design and fabrication strategy for entirely soft, autonomous robots," *Nature,* 2016, 536(7617): 451.

[13] M. Cianchetti, M. Calisti, L. Margheri, et al, "Bioinspired locomotion and grasping in water: The soft eight-arm OCTOPUS robot," *Bioinspiration & Biomimetics,* 2015, 10(3): 035003.

[14] K. Suzumori, S. Endo, T. Kanda, et al, "A bending pneumatic rubber actuator realizing soft-bodied manta swimming robot," *IEEE International Conference on Robotics and Automation (ICRA),* 2007.

[15] M. T. Tolley, R. F. Shepherd, B. Mosadegh, et al, "A resilient, untethered soft robot," *Soft Robotics,* 2014, 1(3): 213-223.

[16] T. G. Hou, X. B. Yang, Y. Aiyama, K. Q. Liu, Z. Y. Wang, T. M. Wang, J. H. Liang, Y. B. Fan, "Design and experiment of a universal two-fingered hand with soft fingertips based on jamming effect," *Mechanism and Machine Theory,* 2019, 133, 706-719.

[17] T. G. Hou, Y. Aiyama, "Universal multi-fingered hand: Soft gripper with jamming effect," *International Conference on Advanced Robotics and Intelligent Systems,* 2016.

[18] J. M. Gosline, M. E. DeMont, "Jet-propelled swimming in squids," *Scientific American,* 1985, 252(1): 96-103.

[19] R. O'Dor, D. M. Webber, "Invertebrate athletes: trade-offs between transport efficiency and power density in cephalopod evolution," *Journal of Experimental Biology,* 1991, 160(1): 93-112.

[20] M.R. Clarke, E.R. Trueman, "Evolution of Buoyancy and Locomotion in recent cephalopods," *Paleontology and neontology of Cephalopods,* 1985, 203-213.

[21] A. Piccirillo, "The Clark Y Airfoil - A historical retrospective," *World Aviation Conference,* 2000.

[22] O. H. Yeoh, "Characterization of elastic properties of carbon-black filled rubber vulcanizates," *Rubber Chemistry and Technology,* 1990, 63: 792-805.

[23] R. W. Ogden, "Large deformation isotropic elasticity-on the correlation of theory and experiment for incompressible rubberlike solids," *Proceedings of the Royal Society of London: Series A,* 1972, 326(1567): 565-584.

[24] H. F. XU, *The basics with aerodynamics,* Beijing: Beijing University of Aeronautics Press, 1987.